PLAXIS LIQUEFACTION MODEL UBC3D-PLM

PLAXIS

Alexandros Petalas

Assistant Researcher, PLAXIS B.V

Vahid Galavi

Researcher, PLAXIS B.V

January 3, 2013

Contents

List of Figures

List of Tables

Abstract

In this report the formulation of the UBC3D constitutive model as implemented in PLAXIS is presented. The UBC3D is a 3-D generalized formulation of the original 2-D UBCSAND model introduced by Puebla et al. (1997). The initial 3-D implementation in PLAXIS was presented by Tsegaye (2010). An improved version is developed by the authors and the final model is presented together with a validation in different monotonic and cyclic stress paths. UBC3D-PLM consists a relatively simple but powerful approach in order to model the onset of the liquefaction phenomenon. In Chapter 1 the main features of the UBC3D-PLM are presented. The model utilises isotropic and simplified kinematic hardening rules for primary and secondary yield surfaces, in order to take into account the effect of soil densification and predict a smooth transition into the liquefied state during undrained cyclic loading. By means of a simplified Rowe stress-dilatancy theory the model is capable of modelling cyclic liquefaction for different stress paths. Post liquecation behaviour of loose sands and cyclic mobility of dense sands can be modelled in terms of a stifness degradation rule. In Chapter 2 the validation of the model in monotonic and cyclic stress paths is discussed. Moreover,the performance of the model in a finite element scheme is investigated and the numerical modelling of a dynamic centrifuge test with PLAXIS 2D Dynamics is presented. The ability of the model to capture the onset of liquefaction is thoroughly discussed. The capabilities and the limitations are highlighted and recommendations for the use of the model are summarized.

Chapter 1

Key Features of UBC3D

The UBC3D-PLM model has been developed by Tsegaye (2010) and implemented as a user-defined model in PLAXIS. It is closely based on the UBCSAND model introduced by Puebla et al. (1997), Beaty and Byrne (1998). The original UBCSAND is a 2-D model developed for prediction of liquefaction in sandy soils. Its formulation is based on classical plasticity theory with a hyperbolic strain hardening rule, based on the Duncan-Chang approach with modifications. The hardening rule relates the mobilized friction angle to the plastic shear strain at a given stress. It contains a 2-D Mohr-Coulomb yield surface and a corresponding non-associated plastic potential function. The flow rule in the model is based on the stress-dilatancy theory developed by Rowe (1962), linearised and simplified according to energy considerations.

The main difference between the UBCSAND model and the UBC3D model is the latter generalized 3-D formulation. The UBC3D model uses the Mohr-Coulomb yield condition in a 3-D principal stress space. Moreover, a modified non-associated plastic potential function based on Drucker-Prager's criterion is used, in order to maintain the assumption of stress-strain coaxiality in the deviatoric plane for a stress path beginning from the isotropic line (Tsegaye, 2010).

Comparing with the previous version of UCB3D implemented in PLAXIS, in the latest version a correction is made in the equation of the plastic multiplier which governs the constitutive relationship between the stresses and strains and higher accuracy is succeeded during monotonic loading. Finally, a soil densification rule added in order to predict a more realistic evolution of excess pore pressures during cyclic loading. This allows the increase of the volumetric strains with a decreasing rate during shearing. Moreover, the bulk modulus of water is depended with the degree of saturation which is specified via PLAXIS input and this user defined model can be used in the Advanced calculation mode of PLAXIS.

The main characteristics of the model as implemented by (Tsegaye, 2010) and modified by the authors are presented in the following sections.

1.1 Yield Surfaces

The UBC3D-PLM model uses the well known Mohr-Coulomb yield function generalized in 3-D principal stress space. In order to understand how the algorithm deals with the complexity of the 3-D representation of the yield surfaces, the full set of the Mohr-Coulomb yield functions are introduced (pressure is positive, tension is positive):

$$f_{1a} = \frac{1}{2}(\sigma_2' - \sigma_3') + \frac{1}{2}(\sigma_2' + \sigma_3')\sin\phi' - c'\cos\phi' \tag{1.1}$$

$$f_{1b} = \frac{1}{2}(\sigma_3' - \sigma_2') + \frac{1}{2}(\sigma_3' + \sigma_2')\sin\phi' - c'\cos\phi' \tag{1.2}$$

$$f_{2a} = \frac{1}{2}(\sigma_3' - \sigma_1') + \frac{1}{2}(\sigma_3' + \sigma_1')\sin\phi' - c'\cos\phi' \tag{1.3}$$

$$f_{2b} = \frac{1}{2}(\sigma_1' - \sigma_3') + \frac{1}{2}(\sigma_1' + \sigma_3')\sin\phi' - c'\cos\phi' \tag{1.4}$$

$$f_{3a} = \frac{1}{2}(\sigma_1' - \sigma_2') + \frac{1}{2}(\sigma_1' + \sigma_2')\sin\phi' - c'\cos\phi' \qquad (1.5)$$

$$f_{3b} = \frac{1}{2}(\sigma_2' - \sigma_1') + \frac{1}{2}(\sigma_2' + \sigma_1')\sin\phi' - c'\cos\phi' \qquad (1.6)$$

The six combinations of the principal stresses in the equations define six planes in 3-D principal stress space. These planes defines the Mohr-Coulomb yield surface as presented in Figure 1.1. The projection of the yield surface in the π -plane is presented in Figure 1.2.
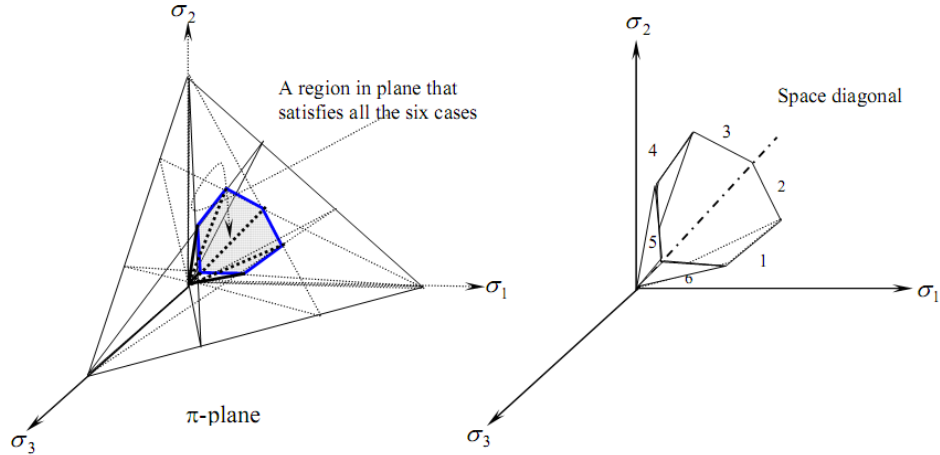
Figure 1.1: The intersection of the six planes and finally the yield surface in 3-D principal stress space. After Tsegaye (2010).

The first step that has to be done by the model is to compute the principal stresses of the stress tensor. This is done after solving the eigenvalue problem. The eigenvalues give the principal stresses and the eigenvectors will be their directions. As far as isotropic behaviour is concerned the directions of the principal stresses are fixed (rotation of the principal stresses is not included in UBC3D-PLM) so the material response is not dependent on the orientation. After the determination of the three principal stresses
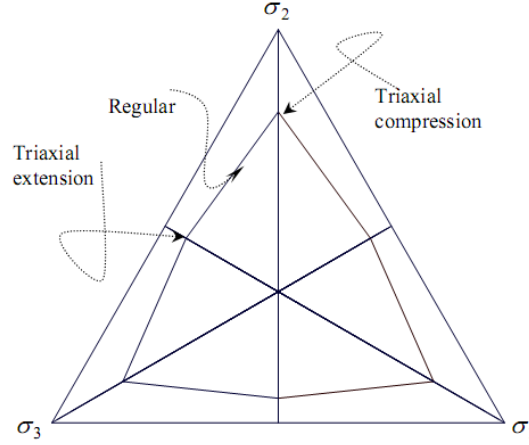
Figure 1.2: Projection of the yield surface in the deviatoric plane. After Tsegaye (2010).

the yield surface has to be defined. Considering any stress path in the generalized 3-D stress space visualized in the deviatoric plane, the yield surface which will be first activated is given by the equation in which the maximum difference between two principal stresses is being used. The critical yield surface in the model is given by Equation 1.7:

$$f_m = \frac{\sigma'_{max} - \sigma'_{min}}{2} - \left(\frac{\sigma'_{max} + \sigma'_{min}}{2} + c' \cot \phi'_p \right) \sin \phi_{mob} \qquad (1.7)$$

The above presented equation is derived by the Mohr-Coulomb failure criterion using the maximum and the minimum principal stress as well as the mobilized friction angle (see Section 1.2). In order to compute Equation 1.7 the principal stresses are sorted as follows:

$$-\sigma_1 \geq -\sigma_2 \geq -\sigma_3 \qquad (1.8)$$

After the sorting and the development of the yield surface, three possible stress paths can be produced by the model, in one of the six parts of the π-plane; triaxial compression, triaxial extension and regular stress path, as depicted in Figure 1.2.

Referred to as the apex term, $c \cot \phi_p$ defines the point where the yield surface intersects the mean effective stress axis (p) (see Figure 1.3). Usually, in granular soils, the cohesion is zero, so the intersection would be located at the origin of the coordinate system (0,0).
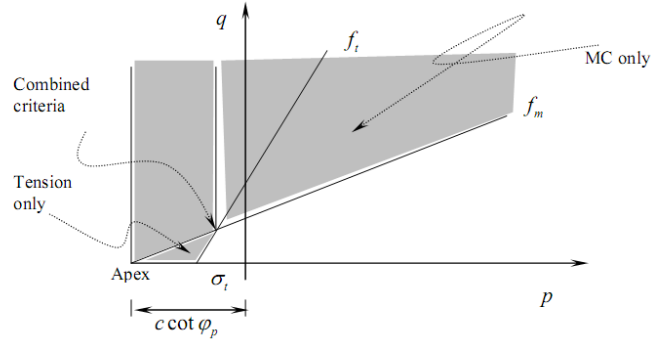
Figure 1.3: Systematization of the yield surfaces in p-q stress space. After Tsegaye (2010).

When the stress state is inside the space defined by the yield surfaces elastic behaviour is assumed. However, once the stress path touches the yield surface plasticity starts to occur. After the reformulation made by the authors the latest version of the UBC3D-PLM has two yield surfaces in order to distinguish between the primary and the secondary loading and to ensure a smooth transition to the liquefied state. This mechanism is better explained in Section 1.5. The elasto-plastic behaviour of the model will be analytically presented in the next paragraph.

1.2   Elasto-plastic Behaviour and Hardening Rule

The elastic behaviour which occurs within the yield surface is governed by a non-linear rule. Two parameters control this non-linear behaviour; the elastic bulk modulus K and the elastic shear modulus G. These two moduli are stress dependent and the relationships are given in the following equations:

$$K = K_B^e P_A \left(\frac{p}{P_{ref}} \right)^{me} \tag{1.9}$$

$$G = K_G^e P_A \left(\frac{p}{P_{ref}} \right)^{ne} \tag{1.10}$$

where K_B^e and K_G^e are the bulk and the shear modulus respectively, at a reference stress level. The factors ne and me are parameters define the rate of stress dependency of stiffness. In the literature, the reference stress level (p_{ref}) is commonly taken as the atmospheric pressure (P_A=100 kPa). Pure elastic behaviour is predicted by the model during the unloading process.

Once the stress state reaches the yield surface, plastic behaviour is predicted as long as the stress point is not going immediately back into the elastic zone. More specifically, plastic hardening based on the principal of strain hardening is used in the model. The hardening rule governs the amount of plastic strain (irrecoverable deformation) as a result of mobilization of the shear strength ($\sin \phi_{mob}$). The mobilized friction angle derived from the Mohr-Coulomb yield criterion (1.7) is given as:

$$\sin \phi_{mob} = \frac{\sigma_1' - \sigma_3'}{\sigma_1' + \sigma_3'} = \frac{t_{mob}}{s'} \tag{1.11}$$

where t_{mob} is the mobilized shear stress and s is the mean effective stress (s).

The hyperbolic hardening rule (Beaty and Byrne, 1998) is presented schematically in Figure 1.4. It relates the increment of the sine of the mobilized friction angle to the plastic shear strain increment as follows (Puebla et al., 1997):

$$\delta \gamma^p = \left(\frac{1}{G^\star} \right) \delta \sin \phi_{mob} \tag{1.12}$$

$$G^\star = k_G^p \left(\frac{p'}{P_A} \right)^{np} \left\{ 1 - \left(\frac{\sin \phi_{mob}}{\sin \phi_{peak}} \right) R_F \right\}^2 \tag{1.13}$$

where k_G^p is the plastic shear modulus number; np is the plastic shear modulus exponent; ϕ_{mob} is the mobilized friction angle, which is defined by the stress ratio; ϕ_{peak} is the peak friction angle; and R_f is the failure ratio n_f/n_{ult}, ranging from 0.5 to 1.0, where n_f is the stress ratio at failure and n_{ult} is the asymptotic stress ratio from the best fit hyperbola.

The hardening rule as reformulated by Tsegaye (2010) in UBC3D-PLM model is given as:
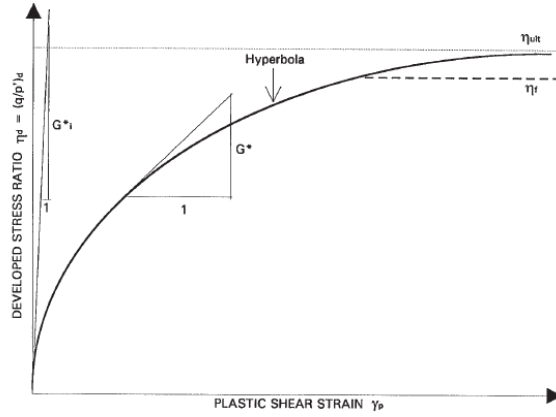
Figure 1.4: The original UBCSAND's Hardening Rule. From Beaty and Byrne (1998)

$$d\sin\phi_{mob} = 1.5 K_G^p \left(\frac{p}{p_A}\right)^{np} \frac{p_A}{p_m} \left(1 - \frac{\sin\phi_{mob}}{sin\phi_{peak}} R_f\right)^2 d\lambda \qquad (1.14)$$

where $d\lambda$ is the plastic strain increment multiplier.

1.3 Plastic Potential Function

The plastic potential function specifies the direction of the plastic strain. A non-associated flow rule based on the Drucker-Prager plastic potential function is used in the UBC3D-PLM (Tsegaye, 2010).

The plastic potential function is formulated as:

8

$$g = q - a \left(p' + c \cot \phi_p \right) \tag{1.15}$$

$$a = \frac{\sqrt{3} \sin \psi_{mob}}{\cos \theta + \frac{\sin \theta \sin \psi}{\sqrt{3}}} \tag{1.16}$$

where θ equals 30° cause the Drucker-Prager surface is fixed in the compression point.

1.4 Flow Rule

In the UBC3D-PLM model the flow rule of the original UBCSAND model is used, which is derived from energy considerations by Puebla et al. (1997). The flow rule used in UBCSAND is based on three observations: 1. there is a unique stress ratio, defined by the constant volume friction angle ϕ_{cv}, for which plastic shear strains do not cause plastic volumetric strains; 2. stress ratios which lie below $\sin \phi_{cv}$ exhibit contractive behaviour, while stress ratios above $\sin \phi_{cv}$ lead to a dilative response; and, 3. the amount of contraction or dilation depends on the difference between the current stress ratio and the stress ratio at $\sin \phi_{cv}$.

The relationship is given as follows:

$$d\epsilon_v^p = \sin \psi_m d\gamma^p \tag{1.17}$$

$$\sin \psi_m = \sin \phi_m - \sin \phi_{cv} \tag{1.18}$$

where, $d\epsilon_v^p$ is the plastic volumetric strain increment and ϕ_{cv} is the constant volume friction angle. A graphical representation of the flow rule is give in Figure 1.5.
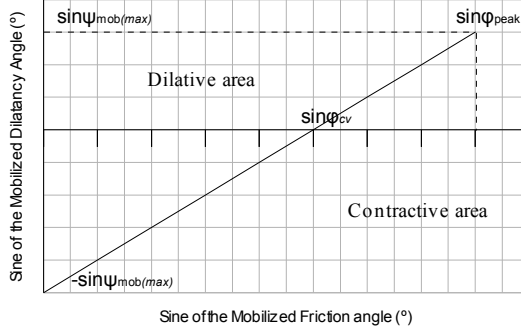
Figure 1.5: Graphical representation of the modified Rowe's flow rule as used in UBC3D-PLM.

1.5 Cyclic Mobility and Stress Reversal

Based on the mobilized friction angle an unloading-reloading criterion is defined in the model as follows:

$$\sin \phi_m^e < \sin \phi_m^0 \textit{(Unloading; elastic behaviour.)} \qquad (1.19)$$

$$\sin \phi_m^e > \sin \phi_m^0 \textit{(Loading or reloading; plastic behaviour.)} \qquad (1.20)$$

The previous mobilized friction angle $(\sin \phi_m^o)$ is memorized from the previous calculation step, while the current one $(\sin \phi_m^e)$ is calculated based on the current stresses. During loading, the friction angle is mobilized, and hardening plasticity occurs. During unloading, pure elastic behaviour is predicted until the stress point reaches the p' axis.

A soil densification rule was introduced in the latest verion of the UBC3D-PLM in order to have higher accuracy in the predicted evolution of the excess pore pressures. A secondary yield surface was introduced in the model for

the secondary loading in order to ensure a smooth transition into the liquefied state of the soil. This enables the distinction between primary and secondary loading.

The secondary yield surface generates less plastic strains compared to the primary yield surface. An isotropic hardening rule is used for the primary yield surface, while a simplified kimematic hardening rule is used for the secondary surface. The plastic shear modulus K_G^p during primary loading is identical with the one entered as input parameter by the user and is used in the hardening rule governing the hardening of the primary yield surface. The plastic shear modulus K_G^p during the secondary loading is formulated as a function of the number of cycles followed during the loading process in order to capture the effect of soil densification during drained shearing reported by many researchers in the literature (Martin et al., 1975).

A simple rule based on stress reversals from loading to unloadind and vise versa is used in order to define the counting of cycles. This leads to an increase of the excess pore pressure during uncdrained cyclic loading with a decreasing rate until the liquefied state is approached.

The modification of the plastic shear modulus during the secondary loading is as follows:

$$K_G^p = K_G^p * \left(4 + \frac{n_{rev}}{2} \right) * hard * fac_{hard} \tag{1.21}$$

where n_{rev} is the number of shear stress reversals from loading to unloading or vice versa, $hard$ is a factor which is correcting the densification rule for loose soils and fac_{hard} is a multiplier which is a user input parameter to adjust the densification rule.

A correction is made in the densification rule for loose sands ($5 \leq N1_{60} \leq 9$) according to the experimental observations and following the formulation of the UBCSAND proposed by Beaty and Byrne (2011) and reported by Naesgaard (2011). The correction rule is as follows:

$$hard = min(1, max(0.5, 0.1N1_{60})) \qquad (1.22)$$

The plastic shear modulus is limited according to the maximum corrected SPT value ($N1_{60}$) of corresponding dense soils (Equation 1.23). The maximum $N1_{60}$ for a very dense soil is defined as 60.

$$K^p_{G,max} = K^e_G * (maxN1^2_{60,max})0.003 + 100 \qquad (1.23)$$

This rule is the result of calibrating a number of direct simple shear tests. Thus, the calibration factor plays a key role when the user wants to model different stress paths (cyclic triaxial tests etc.) and the final value is a matter of judgement according to the most critical stress path for a specific problem. It finally leads to an increase of the excess pore pressure during undrained cyclic loading until the liquefied state is approached. The rate of generation of excess pore pressure decreases by increasing number of cycles which is proven via experiments.

The new yield surfaces are schematically presented in Figure 1.6. In Case a, primary loading occurs during the first half cycle in an arbitrary simple shear test starting from the p' axis. The initial input parameter for the plastic shear modulus K^p_G is used and both yield surfaces expand until the maximum stress state.

In Case b, elastic unloading occurs and the secondary yield surface shrinks until it reaches the isotropic axis where $\sin\phi_{mob}$ is very small. A half cycle is counted. Since an isotropic hardening rule is used for the primary yield surface, it remains at the maximum stress state reached since the beginning of the test.

In Case c secondary loading occurs but with an identical plastic shear modulus as used in primary loading followed by elastic unloading. A full cycle is counted. After the full cycle the densification rule is activated.

In Case d secondary loading occurs with a plastic shear modulus 4.5 times stiffer than used in primary loading. The secondary yield surface expands until it reaches the maximum stress state of the primary yield surface. Then primary loading is predicted again until the new maximum stress state.

Finally, in case e, when the primary yield surface touches the peak stress state (governed by the peak friction angle) the secondary yield surface is deactivated. After the deactivation of the secondary yield surface the primary loading surface is used again.

1.6 Post-liquefaction rule and cyclic mobility

One important issue during the modelling of cyclic liquefaction in sands is the volumetric locking. The evolution of the volumetric strains, after the stress path reaching the yield surface defined by the peak friction angle, becomes constant due to the formulation of the flow rule (in Equation (1.18) $\sin\phi'_{mob}$ becomes $\sin\phi'_p$ and remains constant while $\sin\phi'_{cv}$ is also constant.

Due to this issue the stiffness degradation of the soil due to the post-liquefaction behaviour of loose non-cohesive soils or due to the cyclic mobility of dense non-cohesive sands, which is observed in the experimental studies, cannot be modelled. This limitation is solved in the formulation of the UBC3D-PLM with the implementation of an equation which gradually decreases the plastic shear modulus as a function of the generated plastic deviatoric strain during dilation of the soil element. The stiffness degradation is formulated based on the plastic deviatoric strain related with the dilation of the soil element, due to the deconstruction of the soil skeleton which occurs during dilative behaviour. This leads to the decreased soil stiffness during contraction which follows after the unloading phase. This behaviour is presented in Figure 8 picturing the process of cyclic mobility of a dense sand. The stiffness degradation is computed as follows:

$$K_G^p = K_{G,primary}^p * e^{E_{dil}} \tag{1.24}$$

$$E_{dil} = min(110 * \epsilon_{dil}, fac_{post}) \tag{1.25}$$

where ϵ_{dil} is accumulation of the plastic deviatoric strain which is generated during dilation of the soil element. With the input parameter fac_{post} the value of the exponential multiplier term in the above mentioned equation is limited. The above mentioned behaviour is schematized in Figure 1.7.

1.7 Undrained behaviour in UBC3D-PLM

The undrained behaviour of the soil is treated implicitly by the UBC3D-PLM constitutive model. Therefore, the increment of the pore water pressure is computed at each step of the analysis. Considering a saturated soil specimen, the increments in total stress during loading is given by the following equation:

$$dp = K_u d\epsilon_v \tag{1.26}$$

where K_u is the bulk modulus of the undrained soil and $d\epsilon_v$ the volumetric strain of the soil as a whole.

The effective stress increment can be computed as follows:

$$dp' = K' d\epsilon_v \tag{1.27}$$

where K' is the bulk modulus of the soil skeleton and $d\epsilon_v$ its volumetric strain.

The increments of the pore water pressure is computed with the following equation:

14

$$dp_w = \frac{K_w}{n} d\epsilon_v \qquad (1.28)$$

where K_w is the bulk modulus of the water, n is the soil porosity and $d\epsilon_v$ is the volumetric strain of the fluid.

The relationship between the total stresses, the effective stresses and the pore pressure is assumed according to Terzaghi's theory (Equation 1.29). Moreover, the volumetric compatibility under undrained conditions requires that the equivalent fluid volumetric strain must be equal to the volumetric strain of the soil skeleton. Equation 1.30 is finally derived.

$$dp = dp' + dp_w \qquad (1.29)$$

$$\frac{K_w}{n} = (K_u - K') \qquad (1.30)$$

Once K_w is determined, then the excess pore pressures can be computed in each increment using Equation 1.28. The Poisson's ratio for undrained condition is set as $\nu = 0.495$ implicitly by the model. This value is close to the upper limit (of 0.5) as water is almost incompressible. Using a value of 0.5 is to be avoided as this is known to cause numerical instabilities. Based on this Poisson's ratio the bulk modulus of the undrained soil is computed as follows:

$$K_u = \frac{2G^e(1 + \nu_u)}{3(1 - 2\nu_u)} \qquad (1.31)$$

where G^e is the elastic shear modulus.

The drained bulk modulus of the soil skeleton K' is computed in the same way using the drained Poisson's ratio which is based on the stress dependent stress moduli (Equation 1.32).

$$\nu' = \frac{3K^e - 2G^e}{6K^e + 2G^e} \qquad (1.32)$$

In the latest version of the UBC3D the bulk modulus of water is dependent with the degree of saturation of the soil. This enables the prediction of the pore pressure evolution in unsaturated soils. The bulk modulus of the unsaturated water is defined as follows:

$$K_w unsat = \frac{K_w^{Sat} K_{air}}{S K_{air} + (1-S) K_w^{Sat}} \tag{1.33}$$

where K_w^{Sat} is the bulk modulus of the saturated water and K_{air} is the bulk modulus of air which equals 1 kPa in this implementation having the minimum value. This enables to avoid the generation of pore pressures during modelling a dry sand. under atmospheric pressure. Finally, S is the degree of saturation in the soil.

In this chapter the formulation of the UBC3D-PLM model has been thoroughly discussed. The following chapter presents the validation of the model under triaxial conditions, in order to investigate how well characteristic soil behaviour is captured.

1.8 Parameter selection, summary of the UBC3D input parameters and state variables

In Table 1.8 the input parameters for the UBC3D-PLM model are presented. The main extracting method of the parameters is by fit the experimental curves from element tests. It is crucial to pick the proper element test depends on the stress path which will be the critical during the modelling process. Usually, in earthquake engineering when the onset of liquefaction is the modelling target a drained cyclic direct simple shear test (DSS) is the proper test in order to be able to extract all the parameters for the UBC3D model.

However, in many cases only data from drained triaxial tests are available (CD TxC). As the triaxial test does not involve principal stress rotation, the test data cannot in principal reflect soil response under principal stress

rotation (Vaid et al., 1995). Puebla et al. (1997) proposed a set of equations to be used in the original UBCSAND in order to include the effect of the rotation of principal stresses in terms of stiffness. The equations proposed are derived by experimental observations and fit to the formulation of the UBC3D-PLM constitutive model also. They are derived as follows:

$$For, \quad 0^o \le a_\sigma \le 45^o, \quad then \quad K_G^p = (K_G^p)_0 \{F - (F-1)\cos 2a\} \quad (1.34)$$

$$For, \quad 45^o \le a_\sigma \le 90^o, \quad then \quad K_G^p = (K_G^p)_0 F \quad (1.35)$$

Where:

- and a_σ is the angle between the major principal stress direction and the vertical axis.

- $(K_G^p)_0$ is the plastic modulus number corresponding to $a_\sigma = 0°$ (vertical compression);

- F is the factor of anisotropic plastic response which is less than unity (proposed value 0.317);

With the use of the proposed equations the plastic shear modulus (K_G^p which is proper for modelling the direct simple shear stress path ($a_\sigma = 45°$) is possible if the one suits for triaxial compression is known. Even though with this specific formulation the effect of principal stress rotation in terms of stiffness during plastic hardening can be modelled, the limitations of modelling the inherent and induced anisotropy in the framework of classical plasticity still arise. The proposed equations were derived only in order to overcome the limitation of using parameters generated from triaxial compression tests which is a common procedure in engineering practice.

Finally, some equations for the derivation of the parameters are published by Beaty and Byrne (2011) for the initial calibration of the model

as generic input parameters. These correlations are based on SPT values after calibration of the UBCSAND with proposed analytical solutions and experimental results. The UBC3D-PLM shows a good agreement with the UBCSAND in this stage of development. However, if only the $N1_{60}$ is used for the preliminary parameter selection, the model has to be calibrated with experimental data.

The input parameters of the UBC3D are summarized bellow:

- ϕ_{cv} is the constant volume friction angle;

- ϕ_p is the peak friction angle;

- c is the cohesion of the soil;

- K_B^e is the elastic bulk modulus of the soil in a reference level of 100 kPa. It can be derived from a drained triaxial test with a confining pressure of 100 kPa. When data from a triaxial test with a different confining pressure are available, it can be corrected using Equation 1.9;

- K_G^e is the elastic shear modulus of the soil in a reference level of 100 kPa. It can be related with the K_B^e using the Poison ratio as shown in Equation 1.36;

- K_G^p is the plastic shear modulus and has to be extracted after curve fit;

- me is the elastic bulk modulus index and has a default value of 0.5;

- ne is the elastic shear modulus index and has a default value of 0.5;

- np is the plastic shear modulus index and has a default value of 0.5;

- R_f is the failure ratio n_f/n_{ult} like in Duncan-Chang mode (0.9);

- P_A is the atmospheric pressure;

18

- fac_{hard} is the densification factor. It is a multiplier that controls the scaling of the plastic shear modulus during secondary loading. Above 1 the K_G^p becomes higher and the behaviour stiffer and bellow 1 the K_G^p becomes lower and the behaviour softer;

- $N1_{60}$ is the corrected SPT value of the soil. If this is not known an approximation with relative density can be made as shown in Equation 1.37;

- fac_{post} Fitting parameter to adjust post liquefaction behaviour;

$$\frac{K_B^e}{K_G^e} = \frac{2(1 + \nu')}{3(1 - 2\nu')} \tag{1.36}$$

$$N1_{60} = \frac{RD^2}{15^2} \tag{1.37}$$

$$PPR = \frac{p_i' - p_c'}{p_i} \tag{1.38}$$

where p_i' is the initial effective mean stress and p_c' is the current effective mean stress. When PPR equals 1 then the soil is in a liquefied state. The PPR state variable can show the current status during the calculation whereas the $PPRMAX$ can reveal if the soil had been in the liquefied state even once during the test. The state variable r_u gives similar information as PPR but instead of the effective mean stress the vertical effective stress is used in the equation as shown in Equation 1.39.

$$r_u = \frac{\sigma_{vertical,i}' - \sigma_{vertical,c}'}{\sigma_{vertical,i}'} \tag{1.39}$$

Table 1.1: Input Parameters for the UBC3D.

Name	Symbol	Unit	Method	Default
Constant volume friction angle	ϕ_{cv}	(°)	CD TxC or DSS	-
Peak friction angle	ϕ_p	(°)	CD TxC or DSS	-
Cohesion	c	kPa	CD TxC or DSS	0
Elastic Shear Modulus	K_G^e	-	Curve Fit	-
Elastic Plastic Modulus	K_G^p	-	Curve Fit	-
Elastic Bulk Modulus	K_B^e	-	Curve Fit	-
Elastic Shear Modulus Index	ne	-	Curve Fit	0.5
Elastic Bulk Modulus Index	me	-	Curve Fit	0.5
Plastic Shear Modulus Index	np	-	Curve Fit	0.5
Failure Ratio	R_f	-	Curve Fit	0.9
Atmospheric Pressure	P_A	kPa	Standard Value	100
Tension Cut-off	σ_t	kPa	-	0
Densification Factor	fac_{hard}	-	Curve Fitting	1
SPT value	$N1_{60}$	-	In-Situ Testing	-
Post Liquefaction Factor	fac_{post}	-	Curve Fitting	0.2-1

Table 1.2: State variables of the UBC3D.

| Name	Symbol	Explanation
Mobilized Friction Angle	$sinphi\_mob$	Equation 1.11
Maximum Mobilized Friction Angle	$\max sinphi\_mob$	-
Internal Variable	$etham\_r$	Equals with the $sinphi\_mob$
Number of Cross Over	$xCross$	Number of half cycles
Internal Variable	$dsinphi\_mob$	evolution of $sinphi\_mob$
Confining Factor	$facConf$	Always 1 in this version
Internal Variavle	$PhiPReached$	It is 1 when the ϕ_{peak} is reached
Internal Variable	r_u	Equation 1.39
Initial mean stress	$p0$	In the beginning of the dynamic phase
Pore pressure ratio	PPR	Equation 1.38
Initial vertical stress	$SigV0$	-
Maximum Pore pressure ratio	$PPRMax$	-
Maximum r_u	r_uMax	-
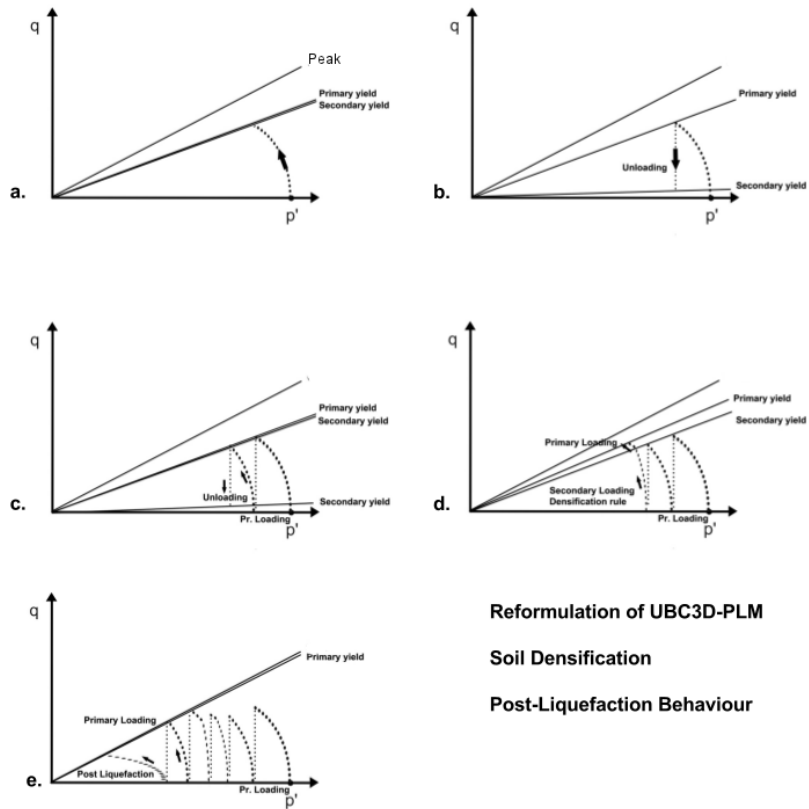
Figure 1.6: Introduction of two yield syrfaces in order to include soil densification, smooth transition in liquefaction state and post-liquefaction behaviour.
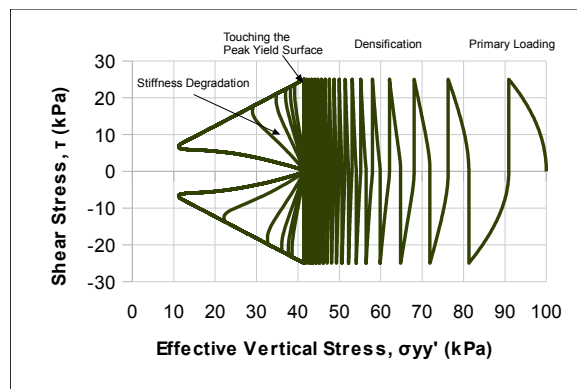
Figure 1.7: Undrained cyclic shear stress path reproduced with UBC3D-PLM for dense sand. Cyclic mobility, stiffness degradation and soil densification are mentioned on the graph.

Chapter 2

Validation of the UBC3D in various stress paths and a finite element scheme

2.1 Validation of the reformulated UBC3D-PLM in monotonic loading

In this section the validation of the UBC3D-PLM under monotonic loading is presented. The numerical modelling of a monotonic triaxial compression (TxC) and a monotonic simple shear test (DSS) are shown and compared with experimental data, as well as with the original UBCSAND as published by Beaty and Byrne (1998).

The parameters used in the tests are extracted from a drained triaxial test. The plastic anisotropic factor is used to modify the plastic shear modulus used in UBC3D-PLM in PLAXIS as proposed by Puebla et al. (1997). The parameters are summarized in Table 2.1.

In Figure 2.1 the results for the numerical modelling of a triaxial compression test are presented. It can be seen that the reproduced soil behaviour from the UBC3D-PLM high accuracy and is in close agreement both with the
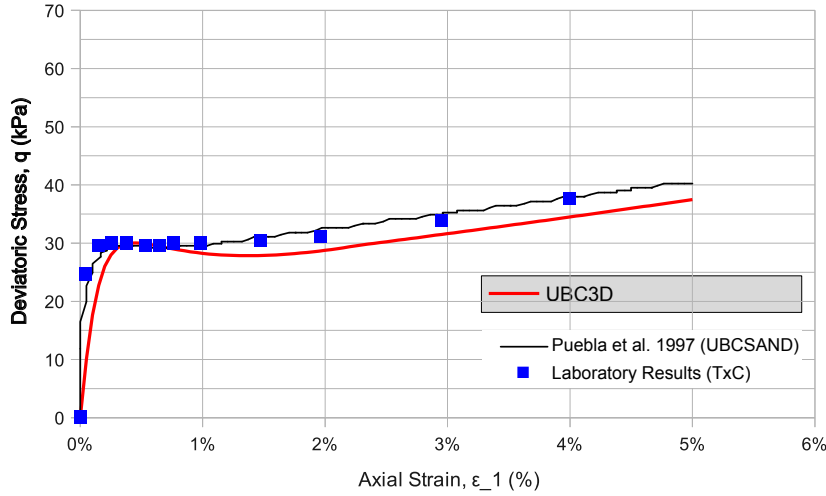
Figure 2.1: Validation of the UBC3D-PLM under monotonic triaxial compression. Undrained behaviour of loose Syncrude sand. Isotropic consolidation with $p' = 100$. The data from the numerical calculation and the experimental result are published by Beaty and Byrne (1998).

experimental data and the results from the original UBCSAND. In Figure 2.2 the results for the numerical calculation of a monotonic direct simple shear test are presented. The UBC3D-PLM model is in good agreement both with the experimental data and the results from the original UBC-SAND for this stress path. The model shows a stiffer undrained hardening behaviour in small strain but this can be improved after a better calibration of the input parameters specifically for the proposed model. In this test the parameters are calibrated based on the original UBCSAND.

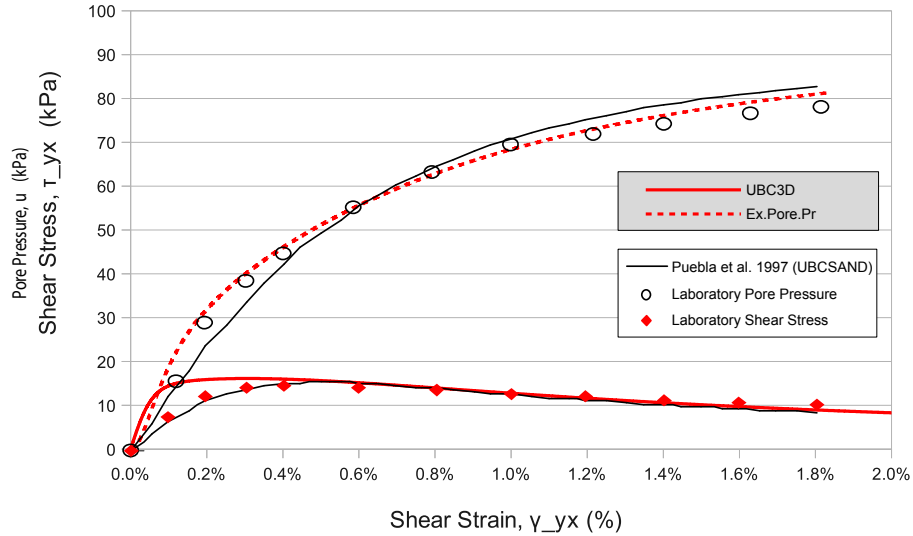It is concluded that the UBC3D can model the undrained behaviour of loose sand with high accuracy.

25

Figure 2.2: Validation of the UBC3D-PLM under monotonic direct simple shear. Undrained behaviour of loose Syncrude sand. Vertical applied stress 100 kPa. The data from the numerical calculation and the experimental result are published by Beaty and Byrne (1998).

2.2 Validation of the UBC3D-PLM in cyclic loading

The behaviour of loose Fraser sand under cyclic direct simple shear is modelled and the numerical results are compared with experimental data as published by Sriskandakumar (2004). The relative density RD of the tested sand is 40 %. Three different shear stress ratios are used (CSR=0.08, 0.1, 0.12) with the same set of parameters. The vertical applied stress is 100 kPa in all cases. The K_0 factor in the numerical calculations is assumed to be 0.46 computed with the well known Jaky formula. Therefore the initial stresses after consolidation in the two horizontal directions equal 46 kPa.

In Figures 2.3, 2.4 and 2.5 the evolution of excess pore pressure in three stress controlled DSS tests are presented. The input parameters are pre-

$\phi_p(°)$	$\phi_c(°)$	K_B^e	K_G^e	$K_G^p(TxC)$	$K_G^p(DSS)$	R_f	F
33.7	33	300	300	310	98.3	0.95	0.317

Table 2.1: Model parameters used to simulate undrained behaviour of loose Syncrude sand (Puebla et al., 1997). The stiffness parameters determined in reference stress level of 100 kPa and are unitless. The R_f and F are unitless parameters.

sented in Table 2.2. Even though modelling the onset of liquefaction in the framework of classical plasticity is very complicated, the UBC3D-PLM constitutive model can reproduce the evolution of excess pore pressures towards cyclic liquefaction with adequate accuracy for three different shear stress ratios using the same set of parameters. The updated formulation of the densification rule is helping the model not to predict very steep evolution of the excess pore pressures in the case of the anisotropic consolidated soil which was reported by Petalas et al. (2012) for previous formulations.

One of the main limitations of the model is presented in the case of the higher shear stress ratio (CSR=0.12). The formulation of the UBC3D-PLM cannot take into account the anisotropic consolidation effects during the primary loading which causes higher evolution of the excess pore pressures during the first full cycle. Due to this issue the UBC3D-PLM predicts a slower evolution for this CSR. The slope of the curve in the experimental results is much steeper during the first two half cycles as can be seen in Figure 2.5. The ability of the UBC3D-PLM of reproducing with high accuracy the cyclic stress paths which are started from the isotropic line was presented by Petalas et al. (2012).

In Figure 2.6 the influence of the post liquefaction formulation can be seen for the case of the lower shear stress ratio (CSR 0.08). The predicted total shear strains are in a good agreement with the experimental results and prove the liquefied state of the soil. The same good agreement in the predicted relationship between the shear stress and the shear strain is ob-

Table 2.2: Input parameters for the validation of the UBC3D-PLM in modelling cyclic element tests and a dynamic centrifuge test.

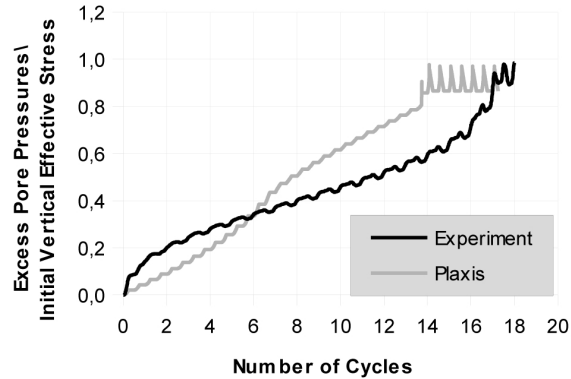|	Cyclic and Dynamic Tests	
Input Parameters	Cyclic DSS	Dynamic Centrifuge
ϕ_p(deg)	33.3	31.2
ϕ_{cv}(deg)	33	34.6
K_B^e(-)	848	720
K_G^e(-)	594	1031
K_G^p(-)	243	700
me and ne(-)	0.5	0.5
np(-)	0.4	0.4
R_f(-)	0.81	0.74
P_A(kPa)	100	100
σ_t(kPa)	0	0
fac_{hard}(-)	0.45	0.45
$N1_{60}$(-)	8	13
fac_{post}(-)	0.01	0.01

Figure 2.3: Evolution of excess pore pressures during simple shearing on Fraser sand (RD=40%). CSR=0.08. σ_v=100 kPa.

served for the other two shear stress ratios as well, still with the same set of parameters.

Finally, in Figure 2.7 a drained strain controlled cyclic direct simple shear test on the same soil is modelled with constant applied strain up to 3%. The first cycle is highlighted. It can be concluded that the constitutive model over-produce hysteretic damping in the system because of the linear elastic unloading rule with constant shear modulus equals G_{max}. This leads to bigger area of the hysteretic loop, which equals with the amount of predicted damping. This fact is well documented in the literature also for the UBCSAND model (Beaty and Byrne, 2011) and is an intrinsic characteristic in the formulation of the model.

In the final section the validation of the reformulated version in a finite element scheme is presented. This gives the opportunity to investigate the limitations of the reformulated version during non-symmetric cycles, under different stress paths during the test and finally to have a clearer opinion on the influence of the K_0 value.
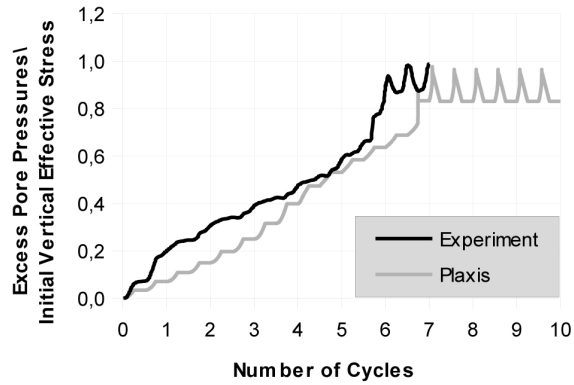
29

Figure 2.4: Evolution of excess pore pressures during simple shearing on Fraser sand (RD=40%). CSR=0.1. σ_v=100 kPa.
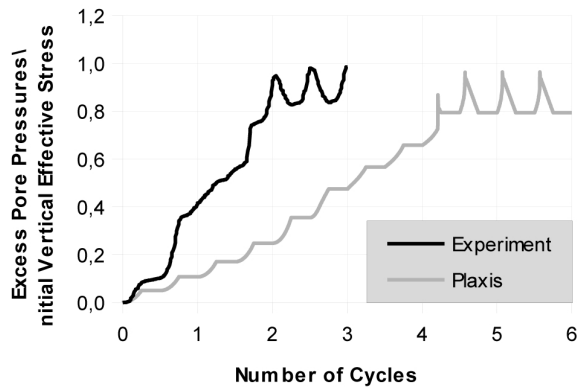

Figure 2.5: Evolution of excess pore pressures during simple shearing on Fraser sand (RD=40%). CSR=0.12. σ_v=100 kPa.
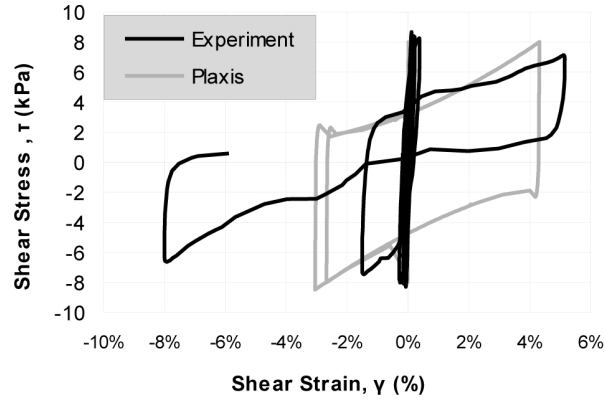
Figure 2.6: Evolution of shear strains during undrained simple shearing. Fraser sand (RD=40%). CSR=0.1. σ_v=100 kPa.
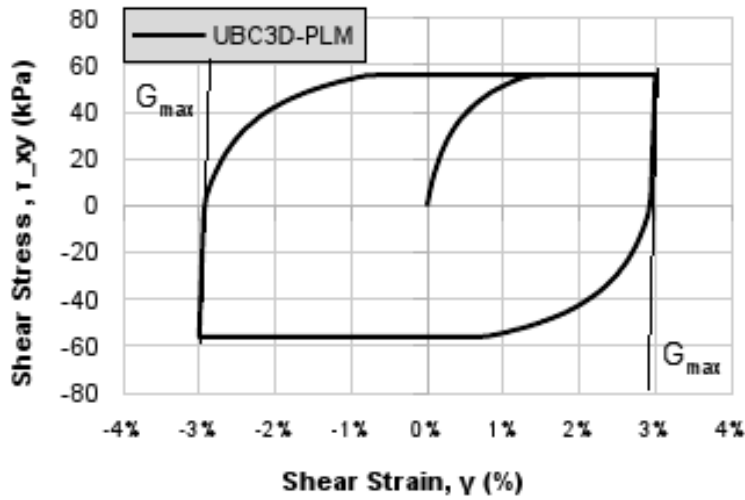

Figure 2.7: Over-produce of hysteretic damping of the UBC3D-PLM constitutive model. The elastic unloading with G_{max} leads to over-produced damping.

2.3   Validation of the UBC3D-PLM in a finite element scheme

A dynamic centrifuge test is modelled with PLAXIS 2D dynamics in order to validate the UBC3D-PLM in a boundary value problem. The numerical results are compared with the experimental results published by Byrne et al. (2004). The input parameters are presented in Table 2.2.

The depth of the sand in the model on prototype scale is 38.1 m. The width does not have any influence in numerical modelling and a 1D soil response is predicted. The total time of the input acceleration is 33 seconds. 50 loading cycles are modelled with constant amplitude of acceleration equal to 1.96 m/s^2.

The results of the predicted evolution of excess pore pressure are presented in Figure 2.8. At 13.1 meters depth the numerical predictions is in a close agreement with the experimental result. The model can predict the onset of liquefaction with adequate accuracy for this depth. However, in the two higher depths, i.e., at 24.8 and 30.8 meters, the model shows inaccuracy during the first loading cycles. It predicts a much steeper evolution of excess pore pressure which lead earlier to the liquefied state compared with the experiment. This issue gets more crucial in the deeper layer.

The influence of the higher relative density in the deeper layer is critical in that case. The UBC3D-PLM cannot take into account the specific feature and the layer is treated as homogeneous. Moreover, the densification of the soil in the two cases is not in close agreement with the experimental results and reveals the complexity of the soil behaviour under undrained cyclic loading. It is concluded from this research that the absence of a stress densification feature in the model leads to a rapid evolution of the pore pressures in the first loading cycles. The effective confining pressure does not influence the behaviour of the current model.
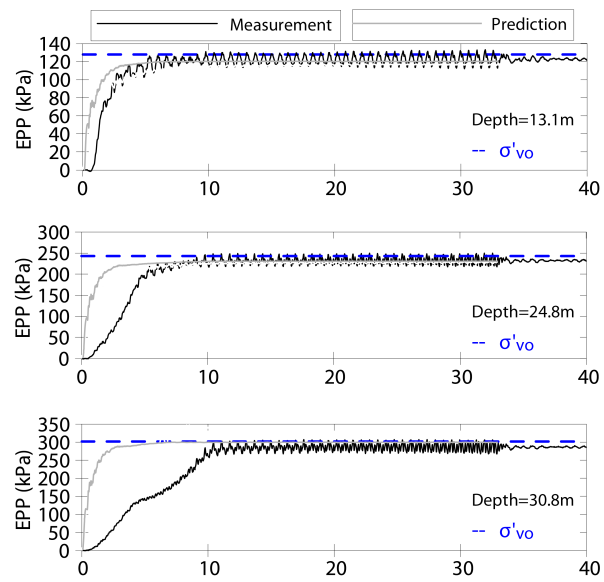
Figure 2.8: Comparison of the predicted evolution of excess pore pressure by the UBC3D with the experimental results published by Byrne et al. (2004).

Bibliography

M. Beaty and P. Byrne. An effective stress model for predicting liquefaction behaviour of sand. *Geotechnical Earthquake Engineering and Soil Dynamics III ASCE Geotechnical Special Publication No.75*, 1:766–777, 1998.

M.H. Beaty and P.M. Byrne. Ubcsand constitutive model version 904ar. *Itasca UDM Web Site*, page 69, 2011.

P. M. Byrne, S. S. Park, M. Beaty, M. Sharp, L. Gonzales, and T. Abdoun. Numerical modelling of dynamic centrifuge tests. *13th World Conference in Earthquake Engineering*, 2004.

G.R. Martin, W.D.L. Finn, and H.B. Seed. Fundamentals of liquefaction under cyclic loading. *Journal of the Geotechnical Engineering Division, ASCE*, 101, 1975.

E. Naesgaard. A hybrid effective stress-total stress procedure for analysing soil embankments subjected to potential liquefaction and flow. *PHD Thesis in the University of British Columbia*, 2011.

A. Petalas, V. Galavi, and R.B.J. Bringkreve. Validation and verification of a practical constitutive model for predicting liquefaction in sands. *Proceedings of the 22nd european young geotechnical engineers conference, Gothenburg, Sweden.*, pages 167–172, 2012.

H. Puebla, M. Byrne, and P. Phillips. Analysis of canlex liquefaction embankments prototype and centrifuge models. *Canadian Geotechnical Journal*, 34:641–657, 1997.

P. W. Rowe. The stress-dilatancy relation for static equilibrium of an assembly of particles in contact. *Proc. R. Soc.*, 269A:500–527, 1962.

S. Sriskandakumar. Cyclic loading response of fraser sand for validation of numerical models simulating centrifuge tests. *Master's thesis, The University of British Columbia, Department of Civil Engineering*, 2004.

A. Tsegaye. Plaxis liqueafaction model. report no. 1. *PLAXIS knowledge base.*, 2010.

Y.P. Vaid, M. Uthayakumar, S. Sivathayalan, P.K. Robertson, and B. Hofmann. Laboratory testing of syncrude sand. *48th Candian Geotechnical Conference, Vancouver, B.C.*, 1:223–232, 1995.